Available online at www.sciencedirect.com

ScienceDirect

Physics Procedia 83 (2016) 1404 – 1414

Physics Procedia

9th International Conference on Photonic Technologies - LANE 2016

Finite element modeling for the structural analysis of Al-Cu laser beam welding

Udo Hartel[a,]*, Alexander Ilin[a], Christoph Bantel[a], Jens Gibmeier[b], Vesselin Michailov[c]

[a]Robert Bosch GmbH, Robert-Bosch-Campus 1, Renningen, 71272, Germany
[b]Karlsruher Institut fuer Technologie, Engelbert-Arnold-Str. 4, Karlsruhe, 76131, Germany
[c]BTU Cottbus-Senftenberg, Konrad-Wachsmann-Allee 17, Cottbus, 03055, Germany

Abstract

Laser beam welding of aluminum and copper (Al-Cu) materials is a cost efficient joining technology to produce e.g. connector elements for battery modules. Distortion low connections can be achieved, which have electrical favorable properties. Numerical simulation of the laser beam welding process of Al-Cu dissimilar materials can provide further insight into principal process mechanisms and mechanical response of the joint parts. In this paper a methodology is introduced to investigate the structural behavior of Al-Cu joints in overlap joint with respect to welding distortions and residual stresses. First the material model of the homogeneous base materials are validated. Next, a generic material model approach is used to simulate the structural behavior of heterogeneous Al-Cu connections.

Peer-review under responsibility of the Bayerisches Laserzentrum GmbH

Keywords: laser beam welding; FEM; material modeling; Al-Cu dissimilar materials; computational welding mechanics

1. Introduction

Since electrification in the automotive industry progresses the demand of lightweight design and tailored material solutions increases. This gives particular emphasis to the application of numerical simulation, e.g. for the joining process of dissimilar material connections like aluminum and copper (Al-Cu). From metallurgical point of view the joining process of dissimilar Al-Cu material combinations poses challenges to welding due to different factors like

* Corresponding author. Tel.: +49-711-811-209-44 .
E-mail address: udo.hartel@de.bosch.com

Peer-review under responsibility of the Bayerisches Laserzentrum GmbH
doi:10.1016/j.phpro.2016.08.147

different solubility of aluminum and copper and absorption, leading to complex weld pool shapes and the formation of brittle intermetallic phases. Improved process strategies have been investigated by *Standfuss* [11] and *Stritt* [12]. The aim of this paper is to evaluate the structural behavior of Al-Cu joints with respect to welding distortions and residual stresses. Numerical simulation provides information about the dimensional stability of the structural parts after welding. Being able to predict the deformation response and taking suitable countermeasures into account can lead to less scrap while manufacturing.

Here we introduce a simulation methodology, based on the Finite-Element-Method (FEM) and experimental investigations to evaluate the structural behavior of laser beam welded Al-Cu joints. The joints consists of pure aluminum (Al99.5) and pure copper (Cu-ETP). For the FEM simulations the commercial software package ABAQUS is used. Welding tests on homogeneous sheet metal specimens and heterogeneous Al-Cu overlap joints form the experimental database of the numerical studies. At first the material models of the homogeneous base materials are validated by means of distortion and residual stress measurements on Al99.5 and Cu-ETP samples. Next, a technique to derive effective material properties for the heterogeneous dissimilar materials joints are presented. In the framework of Computational Welding Mechanics the effective numerical models of the heterogeneous Al-Cu overlap joints are validated by subsequent welding experiments.

2. Experimental Setup

To validate the Finite Element (FE) models of the thermo-mechanical analyzes, welding experiments are carried out on sheet metal specimens for both the homogeneous and heterogeneous materials. The test bench setup for the homogeneous base material models can be seen in Fig. 1. Welding distortions and temperature curves are measured via displacement transducers and thermocouples. In case of the Al-Cu overlap joints, welding distortions are determined optically, based on stochastically distributed grey value patterns on the topside of the specimens (Fig. 2).

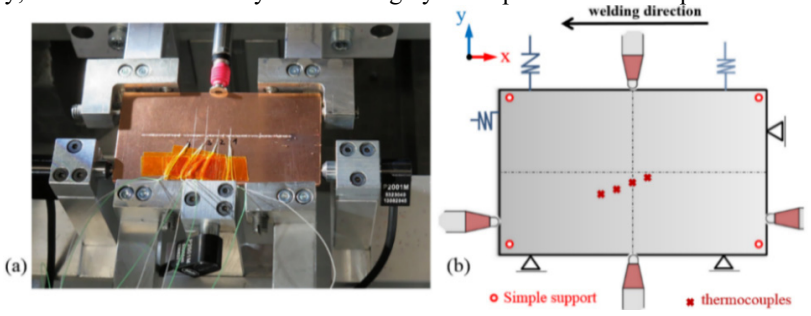

Fig. 1. Test bench setup for the validation of the base material models; (a) experimental setup of e.g. Cu-ETP base material welding experiments; (b) schematic illustration; support of sheet metal specimens for base materials.

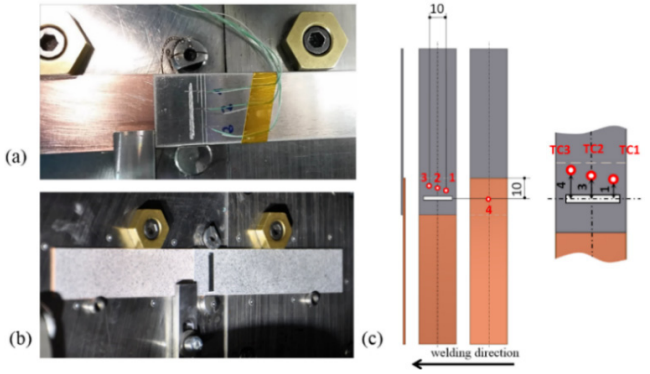

Fig. 2. Test bench setup for Al-Cu overlap joints; (a) positions of thermocouple measurement; (b) applied stochastically distributed pattern for optical measurement of welding distortions; (c) scheme: position of thermocouple for Al-Cu overlap joint configuration.

For laser beam welding a disk laser is used with a wavelength of λ=1030nm. Different weld seam lengths are produced, having a total length from 15mm to 60mm at different focal diameters d_f. A summary of the experimental welding parameters for the base materials and overlap joints is shown in Tab. 1.

Table 1. Summary of welding parameters for welding experiments of Al99.5, Cu-ETP and Al-Cu overlap joints.

material		power	welding speed	focal diameter	weld seam length	shielding gas
		P	v	d_f	l	
		(homogeneous material, sheet metal specimens)				
Al99.5		5000 W	16 m*min^{-1}	400 µm	60 mm	Ar
Cu-ETP		5000 W	16 m*min^{-1}	200 µm	60 mm	Ar
TOP	**BOTTOM**	*(heterogeneous material connections, Al-Cu overlap joint sheet metal specimens)*				
Al99.5	Cu-ETP	1300W	4 m*min^{-1}	50 µm	15 mm	none
Al99.5	Cu-ETP	1200W	8 m*min^{-1}	50 µm	15 mm	none

3. Finite Element Modeling of the Laser Beam Welding Process

3.1. Governing Equations and Constitutive Modeling

To predict residual stresses and welding distortions accurately, information about the temperature field distribution within the heat affected zone is crucial. For structural analysis sequentially coupled thermo-mechanical Finite Element analyzes are performed. The exact physical modeling of the welding process is still a challenging task due to highly nonlinear couplings of different physical domains, thus the complex fluid dynamic processes are often simplified by a heat conduction problem (Eq. 1) with T being the temperature and temperature dependent material properties for density ρ, heat capacity c and thermal conductivity k. q_L is the latent heat due to solid-liquid phase transformation and q_{App} the net heat input of the heat source models.

$$\rho(T)\, c(T)\, \frac{\partial T}{\partial t} = \nabla \cdot (\boldsymbol{k}(T)\, \nabla T) + q_L(T) + q_{App} \tag{1}$$

$$q_{App}^{Ellipsoid} = \begin{cases} q_{App,f}(x,y,z) = \frac{6\sqrt{3}P_L f_f}{abc_f\,\pi\sqrt{\pi}} exp\left(-\frac{3x^2}{a^2}\right) exp\left(-\frac{3y^2}{b^2}\right) exp\left(-\frac{3z^2}{c_f^2}\right), x < 0 \\ q_{App,r}(x,y,z) = \frac{6\sqrt{3}P_L f_r}{abc_r\,\pi\sqrt{\pi}} exp\left(-\frac{3x^2}{a^2}\right) exp\left(-\frac{3y^2}{b^2}\right) exp\left(-\frac{3z^2}{c_r^2}\right), \; x > 0 \end{cases} \tag{2}$$

$$q_{App}^{Cone}(x,y,z) = \frac{3P_L}{\pi z_0 \left[R_K^2 + r_K^2 + r_K R_K\right]} \tag{3}$$

Heat sources are used to model the heat input for laser beam welding. Defined in Eq. 2 and 3 the volumteric power distribution of the double ellipsoidal and conical heat source can be seen according to *Goldak* [3,4]. Where a, b, c_f, c_r r_k, R_k and z_0 are a set of geometrical parameters. f_1 and f_2 (f_1+ f_2=2) represent the energy distribution to the front and rear section of the double ellipsoid and P_L denotes the normal distributed effective laser power. These models are superimposed multiple times for the temperature field analysis of the Al-Cu overlap joints (Fig 3).

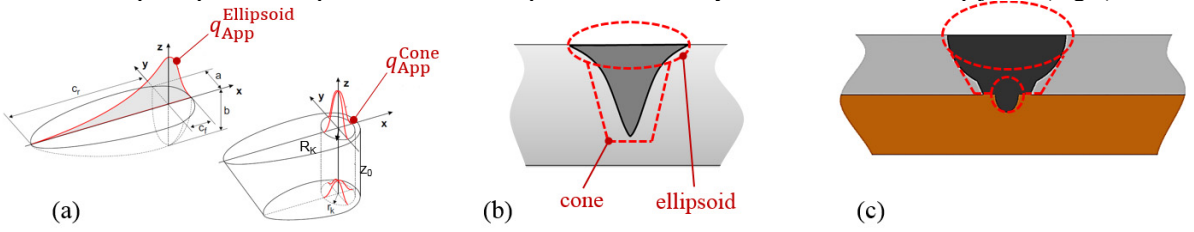

Fig. 3. Heat source models; (a) double ellipsoidal and conical heat source model in accordance to Goldak [3, 4] applied for temperature field reconstruction; (b) heat source model combination for base materials e.g. Al99.5; (c) multiple heat source superposition for overlap joints.

For the mechanical analysis the governing equation is given by the momentum balance. Neglecting intertia forces, this leads to the formulation in Eq. 4 with $\boldsymbol{\sigma}$ being the Cauchy stress tensor and the body forces $\boldsymbol{b}$. The constitutive equation incorporates an incrementally formulated isotropic elasto-plastic material model. The total incremental strain consists of an elastic, plastic and thermal part (Eq. 5). Effects of thermal dilation are included into the constitutive equation (Eq. 6) with d$\boldsymbol{C}$ being the Jacobian matrix, α_{th} thermal expansion coefficient, $\boldsymbol{I}$ the unity tensor and T_{Ref} a reference temperature. Using von Mises J_2 plasticity (Eq. 7) with an associated flow rule - i.e. the plastic strains evolve in normal direction to the Mises yield surface - and isotropic hardening, the flow rule can be written, Eq. 7. With σ_{F} being the temperature dependent yield strength, $\bar{\sigma}$ and $d\bar{\varepsilon}^{pl}$ being the Mises equivalent stress and plastic strain, $\boldsymbol{S}$ the deviatoric stress tensor and $g = d\bar{\sigma}/d\bar{\varepsilon}^{\mathrm{pl}}$ the tangent hardening modulus, see Eq. 8 and 9.

$$\nabla \cdot \boldsymbol{\sigma} + \rho \boldsymbol{b} = \boldsymbol{0} \tag{4}$$

$$d\boldsymbol{\varepsilon} = d\boldsymbol{\varepsilon}^{el} + d\boldsymbol{\varepsilon}^{pl} + d\boldsymbol{\varepsilon}^{th} \tag{5}$$

$$d\boldsymbol{\sigma} = d\boldsymbol{C} : \left[d\boldsymbol{\varepsilon} - d\boldsymbol{\varepsilon}^{th}\right] = d\boldsymbol{C} : \left[d\boldsymbol{\varepsilon} - d\alpha_{th}\boldsymbol{I}\left(T - T_{Ref}\right)\right] \tag{6}$$

$$f(\boldsymbol{\sigma}, \sigma_F) = \sqrt{3\,J_2} - \sigma_F(T) = 0 \tag{7}$$

$$\bar{\sigma} = \sqrt{3\,J_2} = \sqrt{\frac{3}{2}\boldsymbol{S}:\boldsymbol{S}}, \quad d\bar{\varepsilon}^{pl} = \sqrt{\frac{2}{3}d\boldsymbol{\varepsilon}^{pl}:d\boldsymbol{\varepsilon}^{pl}} \tag{8}$$

$$d\boldsymbol{\varepsilon}^{pl} = d\lambda\,\frac{\partial f(\boldsymbol{\sigma})}{\partial \boldsymbol{\sigma}} = \frac{3}{2}\frac{d\bar{\varepsilon}^{pl}}{\bar{\sigma}}\boldsymbol{S} = \frac{3}{2}\frac{d\bar{\sigma}}{g\,\bar{\sigma}}\boldsymbol{S} \tag{9}$$

Within the framework of FEM the weak formulation of the governing equations is used. For detailed derivations of corresponding equations, it shall be refered to *Cardona* [2] or to literature, *Bathe* [1], *Lindgren* [6] and *Radaj* [9].

3.2. Finite Element Models

Hardness measurements (Fig. 4 a,b) show that both base materials exhibit softening while welding due to recrystallization of the microstructure. To model the material's softening a methodology similar to *Ossenbrink* [8] is applied, i.e. temperature and peak temperature dependent flow curves are directly used for the mechanical simulations (Fig. 4 c) and coupled to a numerical annealing procedure. The material data has been determined experimentally by means of a Gleeble testing machine for characteristic laser welding heating and cooling rates.

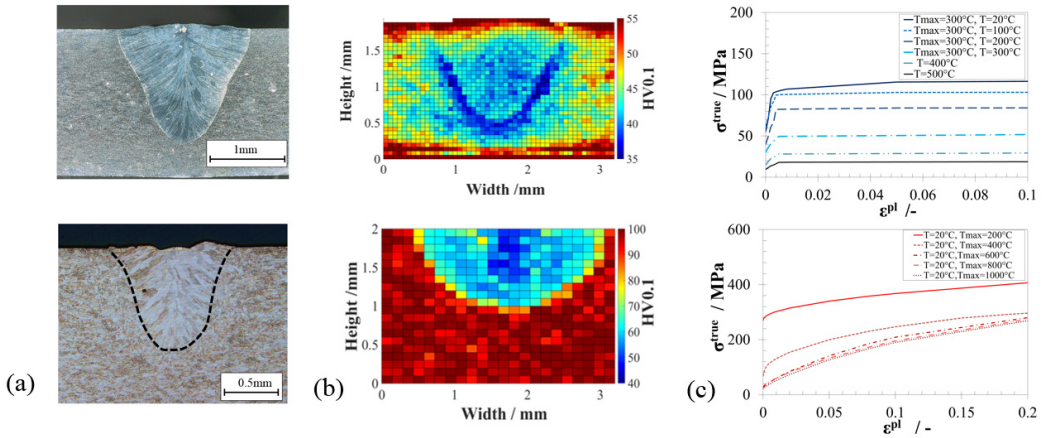

Fig. 4. Softening of base materials Al99.5 and Cu-ETP while laser beam welding, (a) micrographs, (b) hardness measurements, (c) excerpt of temperature and peak temperature dependent flow curves being determined on a Gleeble testing machine.

For thermal simulation thermo-physical material data is implemented into the numerical model. The FE models contain temperature dependent material properties for thermal conductivity, heat capacity and latent heat. A constant convective heat transfer coefficient is assumed for the outer surfaces while cooling. The thermo-physical material data of the Al-Cu overlap joint are derived, based on micrographs, i.e. the amount of molten copper area within the weld seam region is determined. The resulting thermal conductivity values are obtained via linear interpolation between the base material data values. Both welding parameters in Tab. 1 for Al-Cu lead to similar molten areas, therefore the same thermo-physical material data is used. Additionally, thermal and mechanical contact formulation is applied for the numerical modeling of Al-Cu overlap joint gap or penetration behavior.

The temperature field is reconstructed via heat source models, see Fig. 3. The FE models for the base material and the Al-Cu overlap joint can be seen in Fig. 5. The boundary conditions are defined equivalent to the experimental fixations. The FE models include transducer positions (*TP*) as well as checkpoints (*P*) to compare measured and numerically determined welding distortions at discrete points.

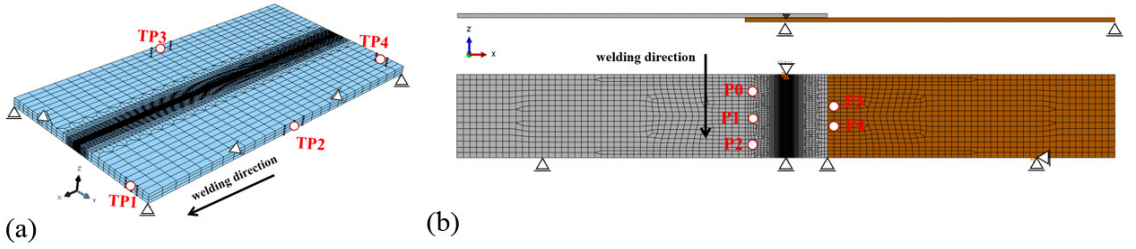

Fig. 5. Finite-Element models for welding simulation, i.e. for carrying out a sequentially coupled thermo-mechanical FE simulation; (a) FE model of base materials with mesh refinement in heat affected zone and positions of displacement transducers *TP*1 to *TP*4; (b) FE model of Al-Cu overlap joint with checkpoint positions P_0 to P_4 for comparing experimental and numerical welding distortions.

3.3. Approaches for Material Modeling of the Al-Cu Dissimilar Material Connections

In this work a phenomenologicalmaterial modeling approach on macro scale is chosen to simulate the mechanical response of the dissimilar material connections in overlap joint. The formation of brittle intermetallic phases is at first neglected and therefore not included. The goal of the study is to compute welding distortions mainly and finally to compare them to welding experiments.

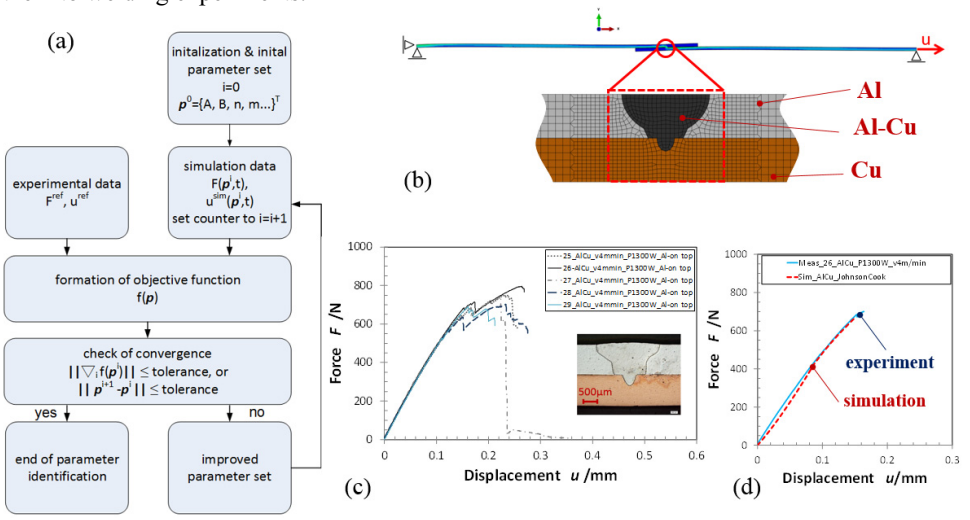

Fig. 6. Parameter identification; (a) scheme of parameter identification for Al-Cu overlap joint shear testing in adaption to Reiger [10]; (b) 2D Al-Cu shear test model; (c) experimental database of shear test force-displacement curves; (d) exemplary result of parameter identification process for Al-Cu overlap joint at *P*=1300W and *v*=4m/min.

$$\sigma_F = [A + B\,(\varepsilon^{pl})^n]\left[1 + C\,ln\left(\frac{\dot{\varepsilon}^{pl}}{\dot{\varepsilon}_0^{pl}}\right)\right]\left[1 - \left(\frac{T - T_{trans}}{T_{melt} - T_{trans}}\right)^m\right] \quad (10)$$

A generic material model approach is selected for the Al-Cu weld seam section, based on the approach of Johnson-Cook (Eq. 10). Here A, B, C, n and m are phenomenological material parameters. T_{melt} and T_{trans} are the melting and the transition temperature. The parameter values of the Johnson Cook model are determined inversely via a parameter identification process (Fig. 6 a). The Johnson-Cook parameters represent the weld seam section's material properties for the cooled down state after welding. Shear tests of the overlap joints form the experimental database for the parameter identification. The Johnson-Cook parameters are calibrated to the ascending force-displacement curves (Fig. 6 d) by using a 2D model, yielding to elasto-plastic material data for the weld.

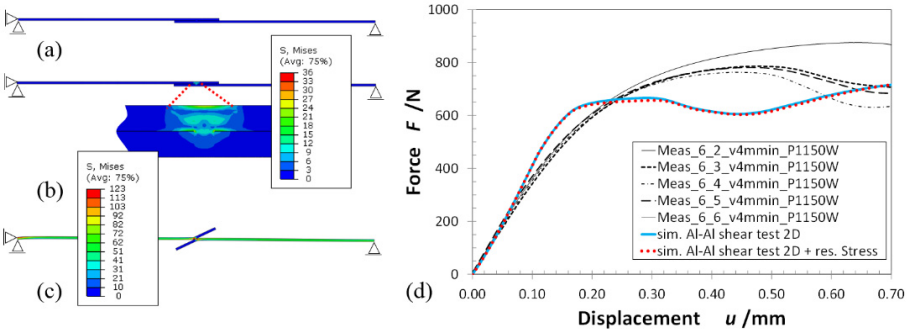

Fig. 7. Numerical shear test simulations of Al-Al overlap joint at P=1150W, v=4m/min of force-displacement curves to verifiy the derivation of material parameter for the dissimilar material section, (a) initial stress free model, (b) pre-stresses model, (c) deformation at numerical shear testing (d) comparison of experimental and numerical force-displacement curves for Al-Al overlap shear tests.

The parameter identification neglects the residual stresses caused by welding. The applicablitiy of the methodology is verified numerically by additional 2D Al–Al overlap joint shear test simulations. Here the thermo-mechanical simulation has been performed prior to the shear test simulation, thus taking into account residual stress state. The resulting curves (Fig. 7) are compared to experimental Al-Al shear tests. The comparison in Fig. 7 shows minor deviations between the two simulation curves. It can be concluded that residual stresses have minor influence, whereas neglecting damage modeling can explain why higher deviations to the experimental results occur.

4. Validation of the Finite Element Models for Welding Simulation

4.1. Validation of the Base Material Models

Heat source models are calibrated, using micrographs of the base materials weld seam cross section area and additional thermocouple measurements (Fig. 8). For Al99.5 a combination of the conical and double ellipsoidal heat sources is applied, whereas for Cu-ETP only the conical source is used.

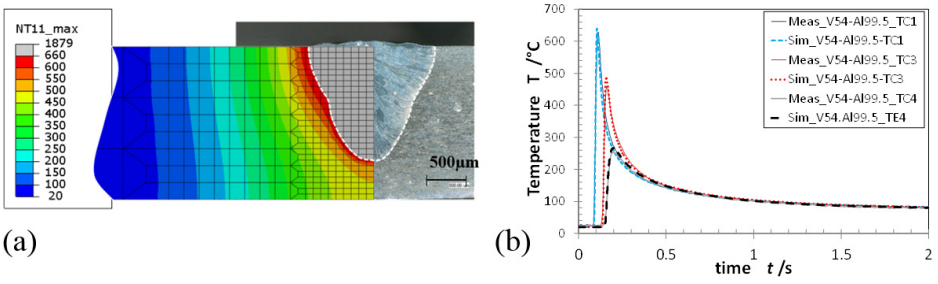

Fig. 8. Heat source model calibration on the example of Al99.5; (a) comparison of computed peak temperatures and fusion line; (b) comparison of experimentally and numerically determined temperature cycles based on thermocouple measurments.

On basis of the temperature field results, welding distortions are computed in a subsequent mechanical analysis. The welding distortions are compared at the displacement transducer positions *TP*3 and *TP*4, see Fig. 9 and 10. The stress-strain data according to Fig. 4 is implemented for the base material FE models.

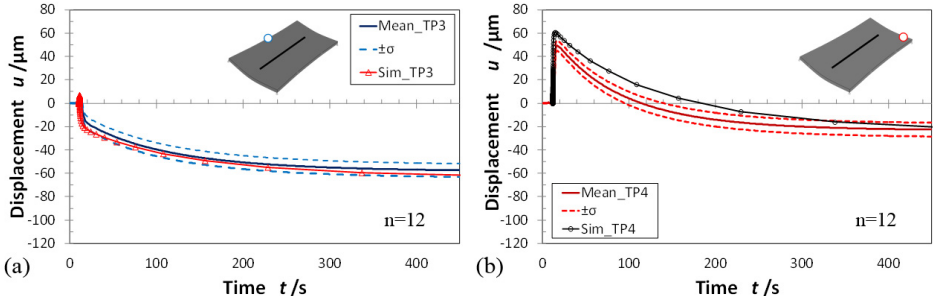

Fig. 9. Comparison of transducer displacements and FE results for Al99.5 at *P*=500W and *v*=16m/min; (a) welding distortion in transverse direction, position *TP*3; (b) welding distortion in longitudinal direction; position *TP*4.

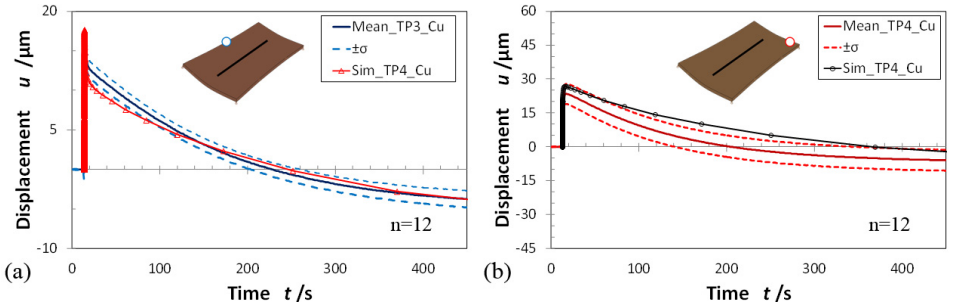

Fig. 10. Comparison of transducer displacements and FE results for Cu-ETP at *P*=500W and *v*=16m/min; (a) welding distortion in transverse direction, position *TP*3; (b) welding distortion in longitudinal direction; position *TP*4.

Besides experimental validation by means of welding distortions, additional measurements of residual stresses and textures are performed. X-ray diffraction measurements are conducted at three different positions on the sheet metal specimens. Orientation distribution functions (ODF) are determined on basis of three incomplete polefigures per measuring position. This data is used to evaluate the residual stress state accurately with respect to exisiting textures (Fig. 11 a).

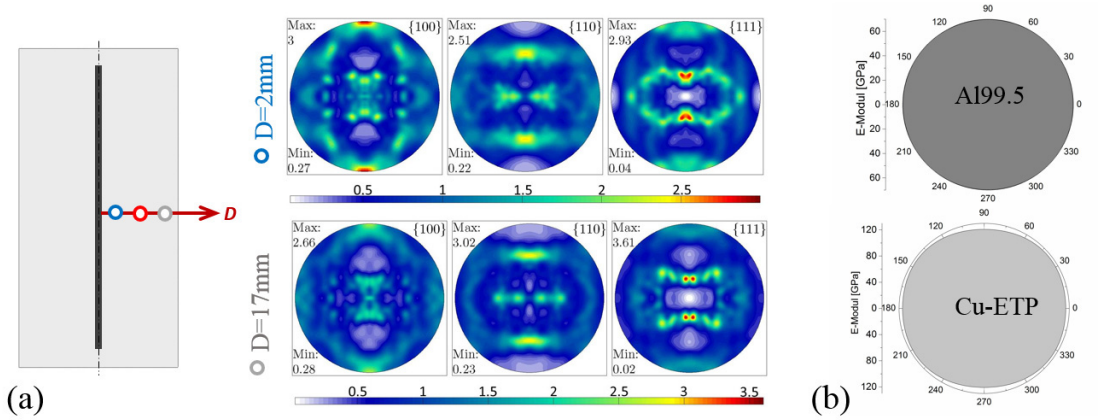

Fig. 11. X-ray residual stress measurement; (a) polefigures backcalculated from ODF for Al99.5 sheet metal specimen at transverse positons 2mm and 17mm from the weld seam center line; (b) in plane distribution of effective Young's Modulus.

For the evaluation of the residual stresses, also including informations of the textures, the $\sin^2(\psi)$-method (*Macherauch* and *Müller* [7]) and the crystallite group method (CG), see *Hauk* and *Vaessen* [5], is used to determine longitudinal residual stresses. $\sin^2(\psi)$-method seems to be applicable due to the relative homogeneous distribution of e.g. Young's Modulus, as can be seen in Fig. 11 b.

The results of the residual stress measurements in longitudinal direction at transversed positions of the specimens are shown in Fig. 12. The measurements are compared to simulation results.

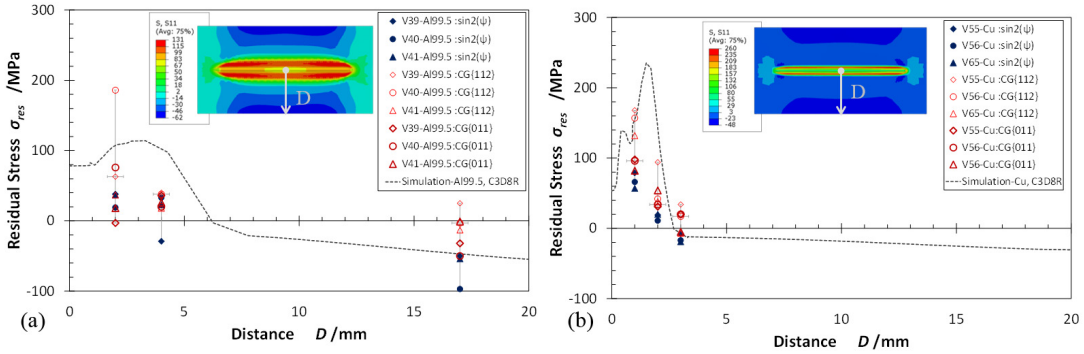

Fig. 12. Comparison of numerical and experimental determined longitudinal residual stresses of base materials, (a) Al99.5, (b) Cu-ETP.

4.2. Comparison of Experimental and Numerical Results for Al-Cu Overlap Joints

Combinations of multiple conical and ellipsoidal heat sources for the temperature field analyzes of the Al-Cu overlap joints are applied. Using FE submodel of the joints, shortens the simulation time for the calibration process (Fig. 13 a). The calibration results are cross-checked on the basis of temperature curves for temperature field analysis, regarding the complete Al-Cu overlap joint model (Fig. 13 b).

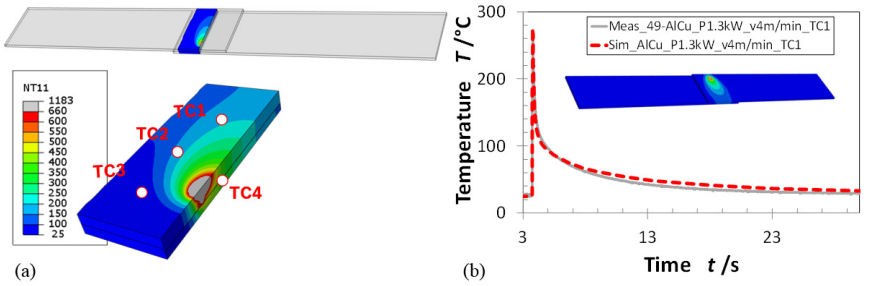

Fig. 13 Al-Cu overlap joint temperature field analysis; (a) FE submodel used for calibration of heat sources with thermocouple points *TC*1 to *TC*4; (b) cross-checking of calibration results on the basis of the complete Al-Cu overlap joint model; comparison of temperature cycles.

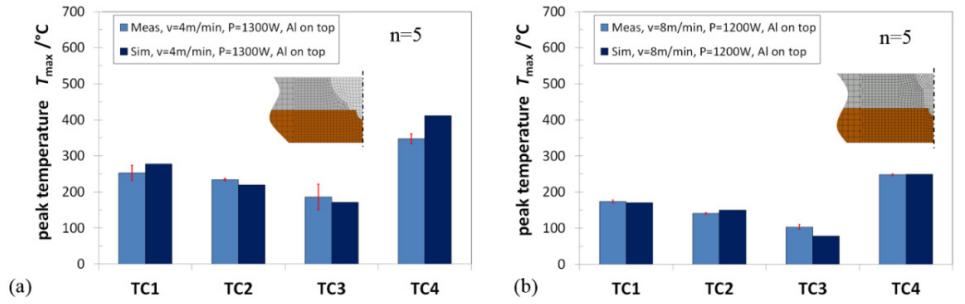

Fig. 14. Results of heat source model calibration for the Al-Cu overlap joint configurations; (a) Al-Cu at P=1300W and v=4m/min; (b) Al-Cu at P=1200W and v=8m/min.

The results of the Al-Cu heat source models calibration for two different welding parameters can be seen in Fig. 14. Fig. 14 presents the comparison of the experimental and numerical determined peak temperatures with respect to thermocouple measurement positions.

While heating up, the structural behavior is governed by the Al99.5 properties, whereas for the cooling phase of the mechanical analysis elasto-plastic material parameters are taken into account, being determined by the Johnson-Cook approach on basis of shear test data. This yields to estimates for the material parameters of the heterogeneous connection. Since approximately 5-6% area fraction of Cu-ETP, being dissolved in the welding, the thermal expansion coefficient of Al99.5 is considered only. Fig. 15 and 16 show the comparison of the experimental and numerical determined welding distortions in x- and y-direction at the checkpoints P_1 and P_2 for the Al-Cu overlap joint setup at two different welding parameters. The distortions are determined via the optical measurement system ARAMIS.

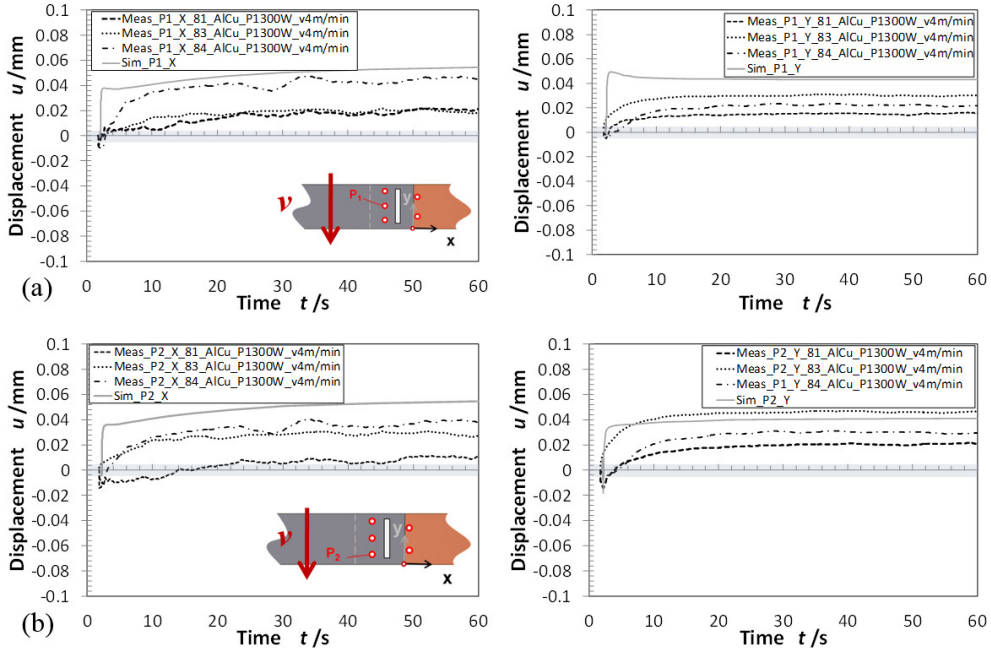

Fig. 15. Comparison of optical measured and numerical determined welding distortions for Al-Cu overlap joint a P=1300W, v=4m/min; (a) welding distortions in x- and y direction at point P_1; (b) welding distortions in x- and y direction at point P_2.

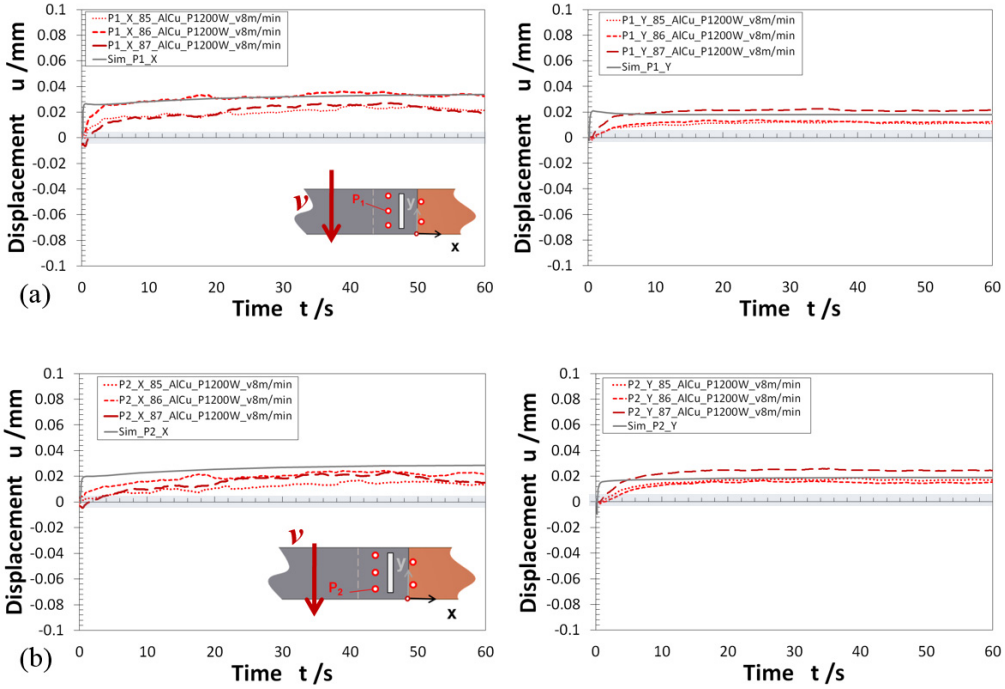

Fig. 16. Comparison of optical measured and numerical determined welding distortions for Al-Cu overlap joint a P=1200W, v=8m/min; (a) welding distortions in x- and y direction at point P_1; (b) welding distortions in x- and y direction at point P_2.

The uncertainty of the optical measurement system is in the range of 10µm. This range is indicated in Fig. 15 and 16 by grey sectors. Despites the assumption made, i.e. using material parameter being calibrated on shear tests data, postulated temperature dependent yield strength and taking into account only the thermal expansion coefficient of Al99.5, the comparison of numerical and experimental results show acceptable deviations.

5. Summary

In this paper a methodology was introduced to investigate the structural behavior of laser beam welded Al-Cu joints. First the material models of the homogeneous based materials have been validated by means of distortions data and measurements of the longitudinal residual stress state. A comparison to experimental results showed good agreement for the base materials Al99.5 and Cu-ETP. Next, material parameters for the Al-Cu heterogenous dissimilar material connections for welding simulation were derived on macro scale. Therefore a generic material model approach was applied, based on the Johnson-Cook approach. Elasto-plastic material data has been derived by shear tests experiments. The final comparison to optical measurement of welding distortions for two Al-Cu overlap joint welding parameters show acceptable deviations.

References

[1] Bathe K.-J., 2002, Finite-Elemente-Methoden, 2. Edition (translated into german), Springer.
[2] Cardona A., Anca A., Risso J., Fachinotti V. D., 2010, Finite element modeling of welding process, Applied Mathematical Modelling 35, 688-707.
[3] Goldak J. A., 2005, Computational Welding Mechanics, Springer.
[4] Goldak J., Bibby M., Moore J., House R. and Patel B., 1986, Computer modeling of heat flow in welds, Metallurgical Transactions B Vol. 17-3, 587-600.
[5] Hauk V., Vaessen G., 1985, Eigenspannungsmessungen in Kristallgruppen texturierter Stähle, Z. Metallkunde 76, 102-105.
[6] Lindgren L. E., 2007, Computational welding mechanics – Thermomechanical and microstructural simulations, Woodhead Publishing, CRC Press.
[7] Macherauch E., Müller P., 1961, Das $\sin^2(\psi)$-Verfahren der röntgenographischen Spannungsmessung, Z. angewandte Physik 13, 305-312.
[8] Ossenbrink R., 2009, Thermomechanische Schweißsimulation unter Berücksichtigung von Gefügeumwandlungen, PhD thesis, BTU Cottbus, Shaker.
[9] Radaj D., 2002, Wärmewirkungen, Eigenspannungen und Verzug beim Schweißen – Rechen- und Messverfahren, Fachbuchreihe Schweißtechnik DVS.
[10] Rieger A., 2005, Zur Parameteridentifikation komplexer Materialmodelle auf Basis realer und virtueller Testdaten, PhD thesis, Universität Stuttgart, Institut für Mechanik (Bauwesen), Lehrstuhl I.
[11] Standfuss J., Kraetzsch M., Klotzbach A, Kaspar J., Brenner B. and Beyer E., 2011, Laser Beam Welding with High-Frequency Beam Oscillation: Welding of Dissimilar Materials with Brilliant Fiber Lasers, Physics Procedia 12, 142-149.
[12]Stritt P., Hagenlocher C., Kizler, Weber R., Rüttimann C. and Graf T., 2014, Laser Spot welding of copper-aluminum joints using a pulsed dual wavelength laser at 532nm and 1064nm, Physics Procedia 56, 759-767.